Hindawi
International Journal of Chemical Engineering
Volume 2023, Article ID 8640288, 13 pages
https://doi.org/10.1155/2023/8640288

Research Article

Copper-Doped Zinc Oxide Nanoparticles: Synthesis, Characterization, and Application for Adsorptive Removal of Toxic Azo Dye

Bandela Sowjanya,[1] Pulipati King ,[1] Meena Vangalapati ,[1] and Venkata Ratnam Myneni [2]

[1]*Department of Chemical Engineering, Andhra University College of Engineering, Visakhapatnam, India*
[2]*Department of Chemical Engineering, Mettu University, Mettu, Ethiopia*

Correspondence should be addressed to Venkata Ratnam Myneni; venkata.rat@meu.edu.et

Received 2 November 2022; Revised 27 November 2022; Accepted 13 December 2022; Published 29 April 2023

Academic Editor: Witold Kwapiński

The goal of this research was to employ copper-doped zinc oxide nanoparticles (Cu/ZnONPs) as an adsorbent to remove the potentially toxic azo dye Congo red (CR). The Cu/ZnONPs were made using a chemical coprecipitation method, and their characteristics were examined using XRD, SEM, EDS, and FTIR methods. The response surface methodology (RSM) central composite design (CCD) is used to optimize the operational parameters' agitation time, adsorbent dosage, solution pH, and initial concentration of CR solution during the adsorption process. The agitation period of 29.48 min, the Cu/ZnONP dosage of 0.301 g/L, the solution pH of 6.96, and the CR initial concentration of 90 mg/L resulted in a maximum CR adsorption of 94.14% and a desirability of 0.976. The kinetic findings fit the pseudo-second-order kinetic equation, and the equilibrium data agreed with the Langmuir isotherm (maximum uptake capacity $q_{max} = 250$ mg/g). During the thermodynamic experiments, endothermic, spontaneous, and physical adsorptions were observed.

1. Introduction

Dyes are used in many different fields, such as textiles, paper, leather, printing, food, plastics, and leather [1, 2]. Some of these dyes are made with chemicals that, even in small amounts, can be harmful to people and animals. Most of these chemicals cause mutations, birth defects, and cancer, which can lead to problems with the kidneys, reproductive system, liver, brain, and central nervous system [3]. Congo red is an example of an azo dye (CR). The nondegradable aromatic group of CR is made up of a biphenyl group in the middle and two naphthalene groups on either side [1]. CR is written as $C_{32}H_{22}N_6Na_2O_6S_2$ and has a molecular weight of 696.7 g/mol. Because CR does not break down and can cause cancer, it is very important to find ways to get rid of it that work and do not cost a lot of money. Adsorption, photodegradation, chemical oxidation, microbiological treatment, and coagulation are some of the most common ways to separate dyes from wastewater [4–9]. A thorough look at the relevant research shows that adsorption is one of the most researched ways to get rid of dyes quickly. This is because it is simple, cheap, and works effectively. Researchers have looked at many different types of adsorbents, both natural and man-made, to see if they can remove dyes and other contaminants from wastewater [10, 11]. Even though these materials are good at getting rid of pollution, they cause a number of problems. Poor adsorption performance and high costs are the main problems.

Researchers all over the world are interested in nanomaterials because their particles are very small, they have very large specific surface areas, and the active places on their surfaces are easily accessible [12]. Scientists are using a variety of nanomaterials that are much better at absorbing dyes and heavy metals. Zinc oxide (ZnO) is a good semiconductor

that can be used in many different ways, such as in solar cells, optical coatings, photo catalysts, and nano-optoelectronic devices [12–14]. It is a good semiconductor because it has a band gap of 3.2 eV and a high excitation binding energy (60 MeV). The ZnO have high electronic conduction, good luminescence, is cheap, and nontoxic. Nanoadsorbents made of zinc oxide have a lot of potential for treating effluent because they are safe, can absorb more, are cheap to make, and can be recycled. Transition metal-doped nanostructures are an effective method for manipulating the energy level surface states of ZnO, which may be further enhanced by changing the doping concentrations of doped materials. Hence, adding other metals to NPs is a great way to alter their properties for the better. Customization is possible by adding transition metals like Fe, Mn, Co, Ni, and Cu to modified ZnO nanostructures. Cu is an excellent doping metal since it is a transition metal with high electrical conductivity and ionic radii similar to ZnO. Researchers discovered that adding Cu to the ZnO matrix alters the microstructure of the ZnO, improving its physical, chemical, and optical characteristics [15–20]. Chemical coprecipitation, sol-gel preparation, thermal breakdown, pulse laser deposition, and hydrothermal processes can all be used to make nanoparticles [19, 20]. The coprecipitation method is especially important and useful because it has many benefits and advantages, such as a low process temperature, low cost, and no need for big equipment.

In recent years, the nanocomposites have attracted substantial interest for a variety of applications, including the adsorption process. Although ZnO nanoparticles are exclusively responsible for excellent pollutant adsorption from wastewater, additional modification of ZnONP with active functional groups speeds up adsorption. Zinc oxide (ZnO) nanoparticles and their doped equivalents have received substantial research in a wide range of scientific domains. Its application in environmental waste treatment is gaining traction due to the low cost and great productivity. The selective removal of nickel ions by different alkaline metals (K^+, Rb^+, and Cs^+)-doped zinc oxide nanoparticles synthesized using various techniques [21]. Klett et al. [22] investigated nickel-doped zinc oxide ($Ni_{0.05}Zn_{0.95}O$) nanoparticles as a potential adsorbent for the removal of methyl orange and tartrazine dyes from an aqueous solution. Experiments revealed that Ni-doped ZnO nanoparticles were extremely effective. A simple coprecipitation approach was used by Saruchi et al. [23] to synthesize ZnO NPs and Mg^{+2}-doped ZnO NPs. The maximal Eosin dye removal values in ZnO NPs and Mg^{+2}-doped ZnO NPs were reported to be 97.9 and 98.4%, respectively. The regeneration efficiencies in ZnO NPs and Mg^{+2}-doped ZnO NPs were 93 and 96% in the first cycle, respectively, and were preserved up to 71 and 81% after the fifth cycle. This proposed that doping ZnO NPs with Mg^{+2} increase their stability and reusability. The removal of malachite green (MG) dye from aqueous medium by vanadium-doped zinc oxide (ZnO : V3%) nanopowder was examined and found to be highly efficient [24].

With this background in mind, the purpose of the present study was to investigate the efficiency of copper-doped zinc oxide nanoparticles (Cu/ZnONPs) towards CR remediation. The Cu/ZnONPs were synthesized by coprecipitating zinc oxide and copper. X-ray diffraction (XRD), scanning electron microscopy (SEM), energy dispersive spectroscopy (EDS), and Fourier transform infrared spectroscopy (FTIR) were used to analyze the Cu/ZnONPs that were produced. In CR adsorption, the agitation time, the Cu/ZnONP dosage, the pH of the solution, and the initial concentration of CR were all investigated as potential process optimization parameters utilizing central composite design (CCD) of response surface methodology (RSM). Furthermore, the kinetics, isotherms, and thermodynamics were also investigated.

2. Materials and Methods

2.1. Synthesis of Cu-Doped ZnO Nanoparticles. A 25 ml solution of 0.5 M $ZnSO_4$ $8H_2O$ was combined with a 25 ml solution of 0.5 M $CuCl_2$ $2H_2O$ and agitated constantly until a clear blue solution was observed. The reaction mixture was treated with 4 M NaOH until the pH reached 11 and the colour transitioned from light blue to dark blue. A blue precipitate emerged after another 2 hrs of heating the reaction mixture at 120°C. The precipitate that formed was allowed to cool at an ambient temperature. The precipitate that formed was filtered, rinsed with deionized water, and dried in an 80°C hot air oven. The resultant material was calcined for 4 hrs in a 400°C furnace [9–11].

2.2. Adsorption Experiments. Adsorption experiments were carried out by varying the agitation time (min), adsorbent dosage (g/L), solution pH, and initial concentrations (mg/L). The contents were shaken for a period of time in a temperature-controlled orbital shaker before being separated by centrifugation for 15 min at 4000 rpm. The dye concentrations were determined using a UV spectrophotometer with a 1 cm quartz cell by detecting maximum absorbance at wavelength 496 nm for CR dye. The pH of the dye solution was determined by a digital pH meter.

The percentage removal of dye was obtained using the following equation:

$$\%\ \text{Removal of dye} = \frac{(C_o - C_e)}{C_e} \times 100. \quad (1)$$

The adsorption capacity of dye or amount of dye adsorbed (q_e) presented in mg/g was determined by using the following mass balance equation:

$$q_e = \frac{(C_o - C_e)}{w}, \quad (2)$$

where C_o and C_e are denoted as initial and equilibrium dye concentrations (mg/L), respectively, and w is the mass of the adsorbent used (g/L) [11].

2.3. Adsorption Isotherm, Kinetics, and Thermodynamics. Adsorption equilibrium studies offer information regarding the adsorbent's capacity. Adsorption isotherms of CR on Cu/ZnONPs were investigated using the Langmuir and Freundlich adsorption models. The Langmuir equation, which is valid for monolayer sorption onto a surface with a limited number of identical sites, is the most extensively used isotherm equation for modelling adsorption data. Equation (3) describes the nonlinear form of the Langmuir model:

$$\frac{C_e}{q_e} = \frac{1}{q_{\max} k_L} + \frac{C_e}{q_{\max}}, \tag{3}$$

where C_e (in mg/L) denotes the concentration equilibrium of the lead ions in the solution, q_e (in mg/g) is the adsorption capacity, $q_{\max}$ (in mg/g) is the maximum adsorption capacity, and k_L (L/mg) is the Langmuir adsorption constant.

The Freundlich isotherm describes the heterogeneous character of adsorption sites with nonuniform energy level distribution. The linear form of the Freundlich isotherm can be expressed as

$$\log(q_e) = n \log(C_e) + \log K_F, \tag{4}$$

where q_e (mg/g) is the amount of adsorbate uptake at equilibrium, C_e (mg/L) is the adsorbate concentration at equilibrium, K_F (mg/g)/(mg/L)^n is the Freundlich constant, and n (dimensionless) is the Freundlich intensity parameter, which indicates the magnitude of the adsorption driving force or the surface heterogeneity.

Kinetic models are used to investigate the rate of adsorption and potential rate-controlling steps. The kinetics of adsorption was investigated using the pseudo-first-order and pseudo-second-order models [11–13]. The pseudo-first-order (PFO) equation can be expressed as

$$\mathrm{In}(q_e - q_t) = -k_1 t + \mathrm{In}(q_e), \tag{5}$$

where t is the time of adsorption and k_1 is the rate constant for PFO.

The pseudo-second-order (PSO) equation can be expressed as

$$\frac{t}{q_t} = \frac{t}{q_e} + \frac{1}{k_2 q_e^2}, \tag{6}$$

where k_2 is the rate constant for PSO.

Adsorption thermodynamic parameters, such as standard free energy change (ΔG), standard enthalpy changes (ΔH), and standard entropy change (ΔS) is characterized as follows: the distribution coefficient K_c of the sorption process, assuming the sorption process, is given by equations (7) and (8):

$$\Delta G = -RT \ln K_c, \tag{7}$$

$$K_c = \frac{C_{\mathrm{ad},e}}{C_e}, \tag{8}$$

where ΔG is the standard free energy change (kJ/mol), T is the temperature in Kelvin, R is the universal gas constant (8.314 mol^{-1}·K^{-1}), $C_{\mathrm{ad},e}$ (mg/L) is the concentration of dye on the adsorbent at equilibrium, and C_e (mg/L) is the equilibrium concentration of dye.

2.4. Response Surface Methodology (RSM). RSM is a beneficial combination of mathematical and statistical methods for assessing quantitative data and their interaction terms from analytical experiments in order to create and solve multivariant equations simultaneously [25, 26]. A well-known RSM design for design improvement is the central composite design (CCD). The CCD is made up of rotating lower-dimensional designs that estimate all linear, quadratic, and two-way interactions. It does not allow for design reduction. They have no corners in the design space. The axial points extend outside the design space box defined by the design's rotatable factorial element. This allows the anticipated response to be estimated with the same variance regardless of direction from the centre of the design area. A preliminary screening was conducted and appropriate ranges of independent process variables. As indicated in Table 1, four independent variables, agitation time (A), Cu/ZnONP dosage (B), solution pH (C), and CR initial concentration (D), were explored using CCD. Stat-Ease Design Expert Software ver.12 was used to predict the CR removal (response) using a 2$^{\mathrm{nd}}$ order polynomial equation.

3. Results and Discussion

3.1. Cu/ZnO NPs Characterization. The XRD was used to analyze the crystalline nature of the samples. The XRD pattern of Cu/ZnO NPs is shown in Figure 1(a). The sample's diffraction peaks all correlate to the hexagonal wurtzite structure of Cu/ZnONPs. The sharpness of the peaks revealed the material's crystallinity. The XRD of the composite sample clearly shows that the ZnO lattice structure is intact even after adding copper ions, which is consistent with previous literature [27]. The surface morphology of Cu/ZnO NPs is depicted in the SEM image in Figure 1(b). The SEM reveals a rather homogenous grain distribution composed of nanoscale particles. The image show that the material's surface is porous and that the particles have agglomerated. According to SEM examination, Cu/ZnO NPs have a significant surface area. This result is compatible with the XRD analysis results. The elemental mapping findings from EDAX (Figure 1(c)) show the presence of C, O, Cu, and Zn. Cu/ZnONPs included 74.30% Zn and 15.516% O by weight, with a Cu attachment of 6.80%. On the ZnO surface, Cu adherence was discovered.

FTIR analysis is used to study the functional groups that exist in the synthesized samples, and Figures 1(d) and 1(e) show the FTIR spectra of Cu/ZnO NPs and Cu/ZnO NPs with CR loaded. The bands found between 3420 and 3800 cm^{-1} indicate the stretching vibration of the -OH groups coupled with zinc ions or might be attributable to water on the surface of the nanoparticles [14–17]. The band noticed at around 1638.6 cm^{-1} and 1423 cm^{-1} are mainly

Table 1: Factors and its levels used for the present study.

Factors	Name	Units	Minimum	Maximum
A	Time	min	10.00	50.00
B	Dosage	g/L	0.1000	0.5000
C	pH		5.00	9.00
D	Concentration	mg/L	30.00	150.00

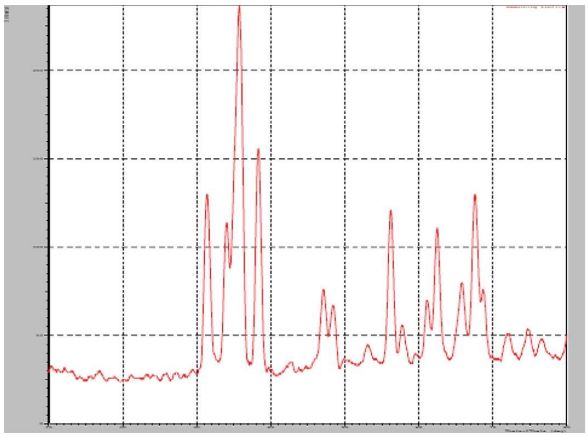

(a)

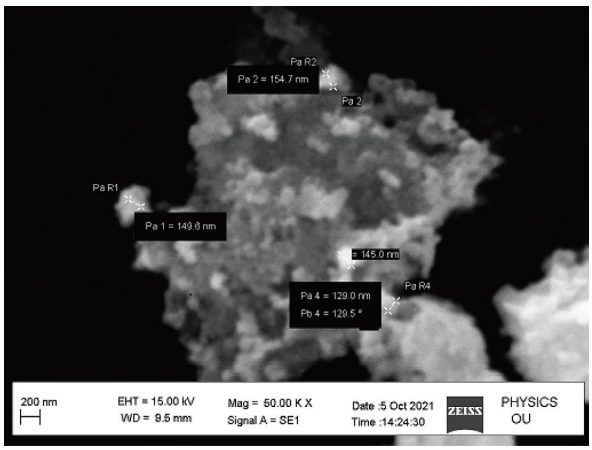

(b)

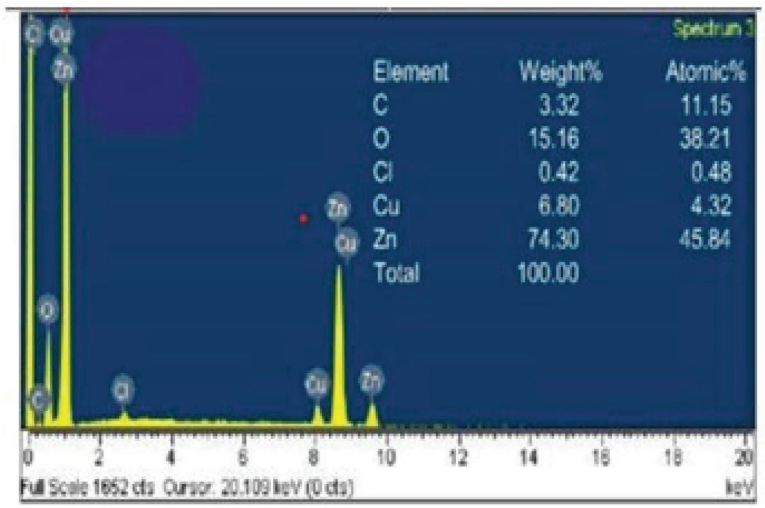

(c)

Figure 1: Continued.

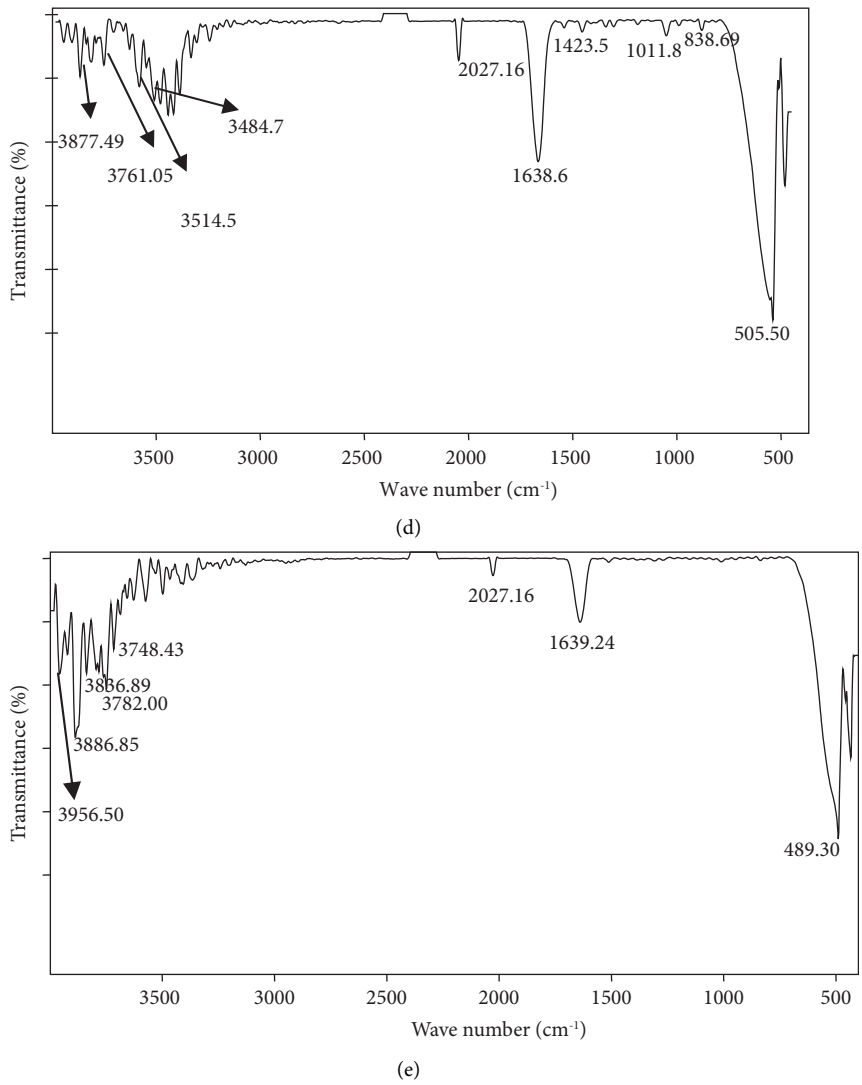

Figure 1: Cu/ZnO NPs characterization: (a) XRD pattern, (b) SEM image, (c) EDS analysis, (d) FT-IR spectra of Cu/ZnO NPs before adsorption, and (e) FT-IR spectra of Cu/ZnO NPs after adsorption of CR.

due to C=O stretching [18–20]. The bands between 1050 and 700 cm^{-1} looked to be caused by ZnO bonding. Adsorption at 511 cm^{-1} is the typical absorption peak of ZnO. The FTIR spectra analysis of Cu/ZnO NPs with CR loaded indicates that all detected functional groups match to metal and that the manufactured materials are in the required form. The interaction with CR caused several of the peaks in the Cu/ZnO NPs FTIR spectra to shift locations or vanish totally. The functional groups of CR might be responsible for the few extra peaks observed in the Cu/ZnO NPs FTIR spectra following loading with Cu/ZnO NPs. According to FTIR analysis, the CR molecules in the aqueous solution were clearly adsorbed by the produced Cu/ZnO NPs.

3.2. Adsorption Experiments. Experiments were carried out in OFAT (one factor at a time) optimization methodology. CR adsorption was carried out at different time intervals (5, 10, 15, 20, 25, 30, 35, 40, 45, 50, 55, and 60 min), while holding all other variables constant, such as adsorbent dosage 0.3 g/L, pH 6, and temperature 303 K. Initially, the adsorption was very fast, after 30 min, the removal rate remained constant. The impact of adsorbent dose on CR dye adsorption on Cu/ZnO NPs was investigated in the range of 0.1 to 0.8 g/L, with all other parameters such as agitation period 30 min, pH 6, and temperature 303 K held constant. The maximum CR removal of 56.1%, when the adsorbent dose increased, is 0.3 g/L. The impact of pH on the removal of CR dye by Cu/ZnO NPs was studied by altering the pH of CR from 4.0 to 9.0. The optimum pH is considered as 7.0 for CR adsorption. The influence of initial concentration on the adsorption of CR dye on the ZnONPs was investigated in the range of initial concentrations from 10 to 100 mg/L, keeping all the remaining parameters, such as agitation time 30 min, pH 7, and temperature 303 K as constants. At 100 mg/L, the maximum CR removal of 90.6% was recorded.

3.3. Response Surface Methodology (RSM). Central composite design (CCD) was applied based on 30 experimental runs with four independent variables, agitation time (A), Cu/ZnONP dosage (B), solution pH (C), and CR initial concentration (D), and it was conducted to investigate their main interaction contribution on CR adsorption. Replicates were used to avoid experimental errors. The analysis of variance (ANOVA) was used to realize the diagnostics checking test for adequacy of the proposed model based on the Fishers F test. The regression coefficient (R^2) indicates the amount of variation around the mean explained by the model. The coded and uncoded levels of independent factors according to 30 experiments corresponding to CCD along their responses are shown in Table 2. The quadratic model in terms of coded factors is expressed as the following equation:

$$\begin{aligned} CR \text{ removal} = {} & -126.57 - 1.40217\,\text{Time} + 434.4\,\text{Dosage} + 40.69667\text{pH} + 0.770611\,\text{Concentration} + 0.64\text{Time} * \text{Dosage} \\ & + 0.480250\text{Time} * \text{pH} + 0.006250\text{Time} * \text{Concentration} - 12.575\text{Dosage} * \text{pH} - 0.31\text{Dosage} * \text{Concentration} \\ & - 0.015583\text{pH} * \text{Concentration} - 0.045771\text{Time}^2 - 560.95833\text{Dosage}^2 - 3.56458\text{pH}^2 - 0.004238\text{Concentration}^2. \end{aligned} \tag{9}$$

3.3.1. Analysis of Variance (ANOVA). The Model F value of 71.69 indicates that the model is statistically significant (Table 3). There is a 0.01% probability that such a large F value occurs as a result of noise. P values less than 0.0500 indicate the existence of significant model terms. AC, AD, BC, BD, A^2, B^2, C^2, and D^2 are the significant model terms in this situation. The F value for lack of fit is 0.2268, indicating that the lack of fit is not significant in comparison to the pure error. A negligible lack of fit is desirable. The predicted R^2 of 0.9278 is reasonably close to the adjusted R^2 of 0.9715 (Table 4). The signal-to-noise ratio is determined by Adeq Precision. A ratio greater than 4 is preferred, so that the design space can be navigated.

3.3.2. Response Surface Plots and Interaction between the Parameters for CR Adsorption. To assess CR adsorption, 3D response plots were used to find the experimental data, and the influence of factors such as agitation time, Cu/ZnONP dose, solution pH, and initial CR concentration was seen. As shown in Figures 2(a) and 2(b), increasing the contact time had a positive effect on total CR adsorption. This might be due to the fact that the adsorbent surface initially had a significant number of active sites that were later occupied by dye molecules. Furthermore, the plots showed that when the contact period was extended beyond 30 min, the CR adsorption remained generally consistent. Solution pH has a considerable influence on CR adsorption, as seen in Figures 2(a) and 2(c). The CR adsorption increases from 4.0 to 7.0 and then falls at basic solutions. At decreasing pH, $-NH_2$ groups in CR are protonated and become $-NH^{3+}$. The same positive charge causes a repulsive contact between the surface of Cu/ZnONP and the CR molecule, resulting in a reduction in the % removal of CR dye. Similarly, due to electrostatic repulsion between negatively charged adsorbent surfaces and negatively charged dye ions, alkaline solutions are unfavourable for CR adsorption. The initial CR concentration is another important factor influencing adsorption. When the initial CR concentration was raised, a linear impact was seen that was statistically significant. This suggests that raising the initial CR concentration causes an increase in adsorption, as illustrated in Figures 2(b) and 2(d).

3.3.3. Optimization. The goal of this study is to optimize responsiveness across a collection of factors. The design expert program chooses the variables required to get the best results. As shown in Figure 3, optimal settings of agitation time is 29.48 min, Cu/ZnONP dose is 0.301 g/L, solution pH is 6.96, and CR initial concentration is 90 mg/L produced in maximum CR adsorption of 94.14% with a desirability of 0.976. The experimental response achieved under the provided ideal conditions confirmed the projected CR removal.

3.4. Adsorption Kinetics. In order to pattern diffusion of dyes into the adsorbent particles and providing some more insights into the reaction pathways, it is essential to choose an appropriate model for the analysis of data [25, 26]. The adsorption kinetics of CR dye onto the Cu/ZnONP was investigated via pseudo-first-order and pseudo-second-order. The fitted plots of these adsorption kinetic models are shown in Figures 4(a) and 4(b) and these kinetic parameters are summarized in Table 5. The validity of each model is checked by the corresponding correlation coefficients (R^2). In case of the pseudo-first-order kinetic model, the overall adsorption rate is directly proportional to the driving force, which is the difference between the initial and equilibrium concentrations of the dye. Comparison of correlation coefficients of pseudo-first-order ($R^2 = 0.987$) and pseudo-second-order ($R^2 = 0.996$) kinetic models show that pseudo-second-order best describes the mechanism and the rate uptake of CR dye on Cu/ZnO NPs. It can be concluded that the adsorption system is a chemical process involving electron sharing or electron transfer [13, 14].

3.5. Adsorption Isotherms. Adsorption isotherms aid in the identification of the process mechanism, adsorbent characteristics, and adsorbate-adsorbent interactions [28–30]. Thus, equilibrium data correlation is critical for adsorption data interpretation and prediction. Figures 4(c) and 4(d) illustrate the fitting charts for the Langmuir and Freundlich isotherm models. The Langmuir model assumes that the number of adsorption sites is fixed, a monolayer surface

Table 2: Designed variables and the response using CCD.

Run	Time (min)	Dosage (g/L)	pH	Initial concentration (mg/L)	Response (% CR removal)
1	10	0.3	7	90	77.5
2	30	0.3	7	90	94.8
3	20	0.2	6	60	81.56
4	20	0.2	8	60	74.4
5	20	0.4	8	120	66.8
6	40	0.2	6	120	71.6
7	30	0.3	9	90	79.6
8	40	0.4	8	120	79.7
9	20	0.2	6	120	80.6
10	30	0.3	7	90	94.8
11	30	0.3	7	90	94.8
12	30	0.3	7	90	93.4
13	30	0.3	7	30	79.5
14	20	0.4	8	60	73.48
15	20	0.4	6	60	85.2
16	20	0.2	8	120	73.06
17	40	0.2	8	60	80.5
18	30	0.1	7	90	70.5
19	40	0.4	8	60	80.8
20	30	0.5	7	90	73.24
21	20	0.4	6	120	77.6
22	40	0.4	6	60	70.24
23	30	0.3	7	90	94.8
24	30	0.3	7	150	78.6
25	50	0.3	7	90	74.5
26	30	0.3	5	90	80.5
27	30	0.3	7	90	92.2
28	40	0.4	6	120	76.6
29	40	0.2	6	60	67.24
30	40	0.2	8	120	84.3

Table 3: ANOVA for the quadratic model.

Source	Sum of squares	d*f*	Mean square	*F* value	*p* value	
Model	2040.47	14	145.75	71.69	<0.0001	Significant
A-time	2.48	1	2.48	1.22	0.2865	
B-dosage	0.2904	1	0.2904	0.1429	0.7108	
C-pH	0.0150	1	0.0150	0.0074	0.9327	
D-concentration	1.03	1	1.03	0.5042	0.4885	
AB	6.55	1	6.55	3.22	0.0927	
AC	369.02	1	369.02	181.53	<0.0001	
AD	56.25	1	56.25	27.67	<0.0001	
BC	25.30	1	25.30	12.45	0.0030	
BD	13.84	1	13.84	6.81	0.0197	
CD	3.50	1	3.50	1.72	0.2094	
A^2	574.62	1	574.62	282.66	<0.0001	
B^2	863.11	1	863.11	424.57	<0.0001	
C^2	348.51	1	348.51	171.44	<0.0001	
D^2	399.11	1	399.11	196.33	<0.0001	
Residual	30.49	15	2.03			
Lack of fit	24.44	10	2.44	2.02	0.2268	Not significant
Pure error	6.05	5	1.21			
Cor total	2070.97	29				

forms, there is no interaction between adsorbate molecules, and the adsorbent surface is homogeneous. The figures show that the Langmuir model can better represent the adsorption data. The Langmuir model may be used to compute the monolayer adsorption capacity on the homogeneous surface, which is 250 mg/g for CR

Table 4: Fit statistics.

Std. dev.	1.43
Mean	80.08
C.V. (%)	1.78
R^2	0.9853
Adjusted R^2	0.9715
Predicted R^2	0.9278
Adeq precision	27.5626

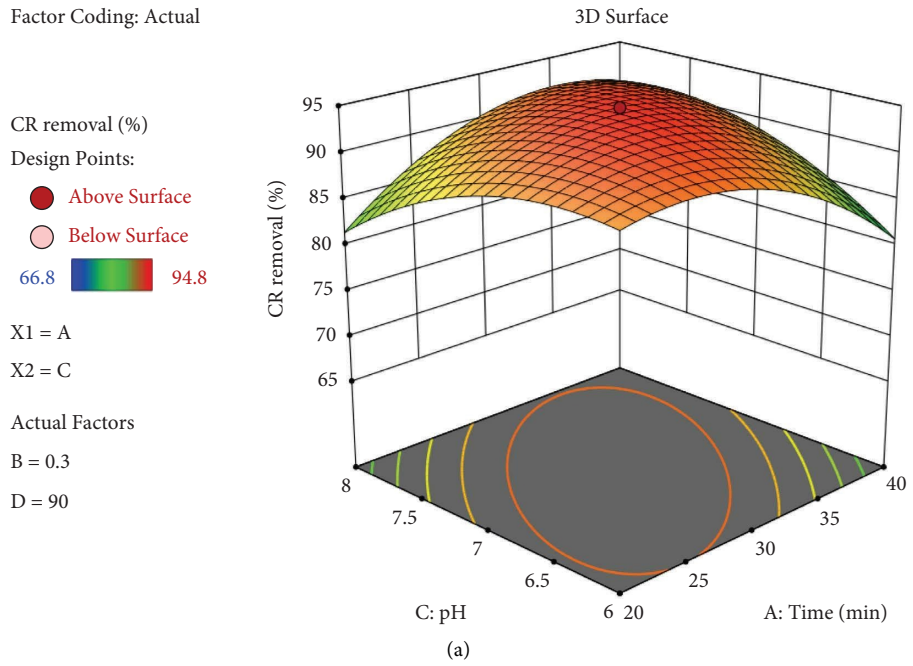

(a)

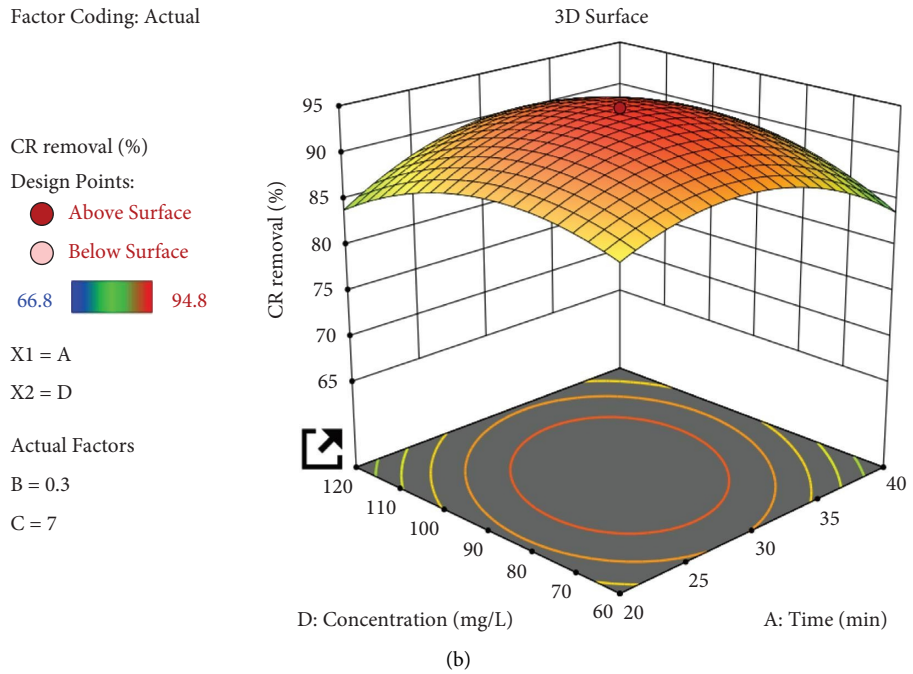

(b)

Figure 2: Continued.

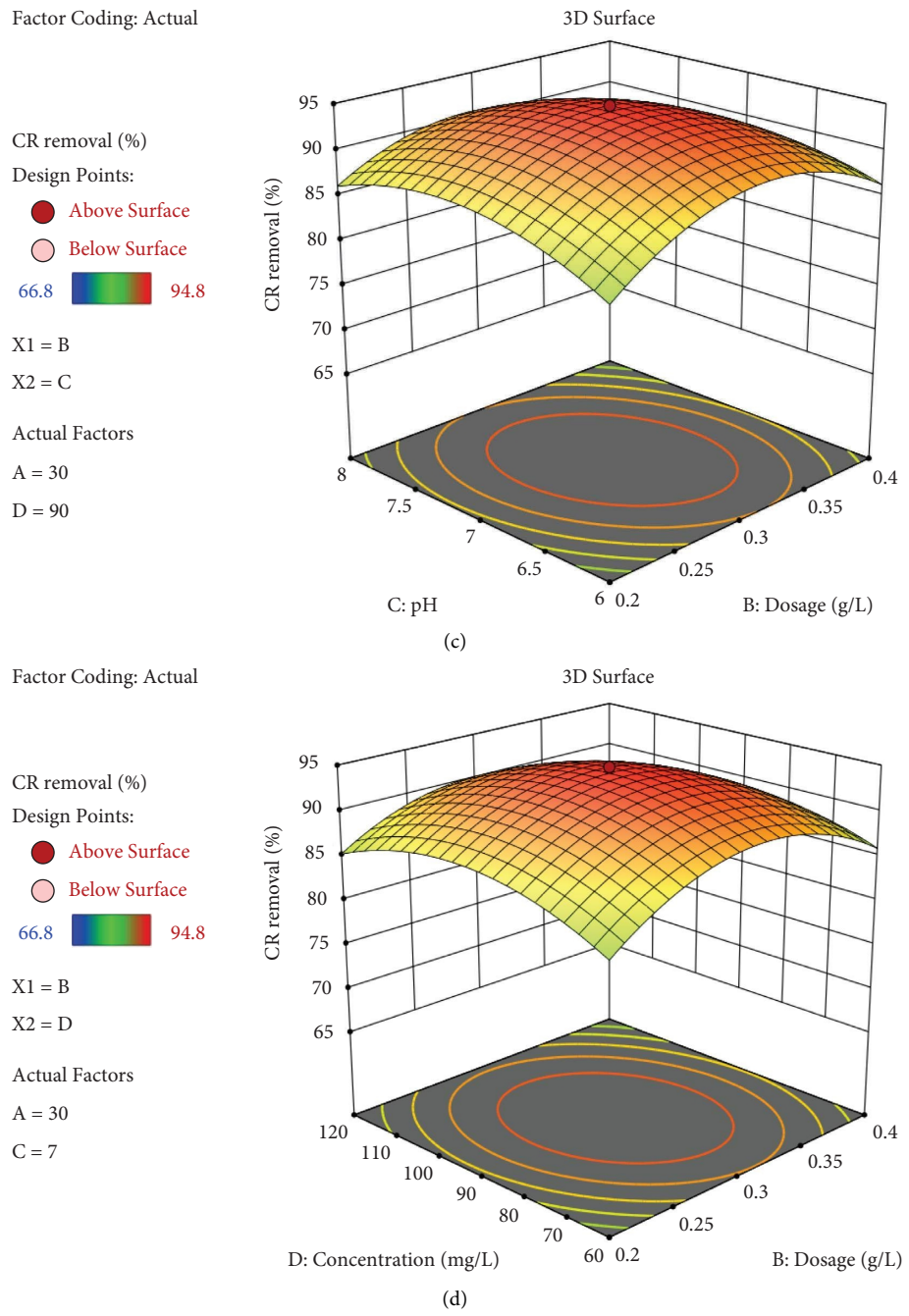

Figure 2: (a) Response surface plots for adsorption of CR onto Cu/ZnONP: interactive effects of pH and time, (b) response surface plots for adsorption of CR onto Cu/ZnONP: interactive effects of time and concentration, (c) response surface plots for adsorption of CR onto Cu/ZnONP: interactive effects of pH and dosage, and (d) response surface plots for adsorption of CR onto Cu/ZnONP: interactive effects of dosage and concentration.

dye. This estimate matches closely with the experimental adsorption capacity. The Langmuir constant k_L is calculated to be 0.104712 L/mg. The Freundlich isotherm, which implies multilayer adsorption with intermolecular interactions, predicts that dye limits on the adsorbent surface rise as dye concentration in the solution increases. The Freundlich constant (n) value of 0.4797 (between 0 and 1), which was deemed the adsorption intensity factor or surface heterogeneity, suggests favorable adsorption.

3.6. Adsorption Thermodynamics. The results obtained from Figure 4(e) can be used to calculate the thermodynamic parameters. The thermodynamic parameters measured are presented in Table 6. The negative values of ΔG at various temperatures suggest that the adsorption process was spontaneous and thermodynamically feasible [31–33]. The ΔG values slightly decrease with the increasing temperature, implying that more dye was adsorbed onto the adsorbent surface at higher temperatures. Hence, the adsorption of CR dye is favoured at relatively higher temperatures. The positive values of ΔH and ΔS

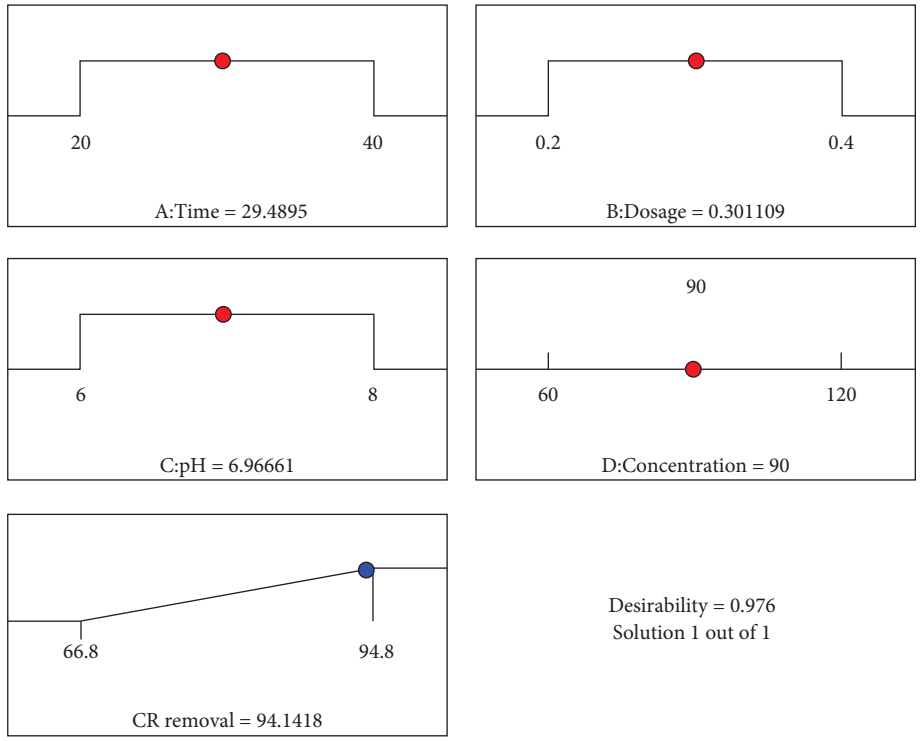

Figure 3: Ramp plot of optimization.

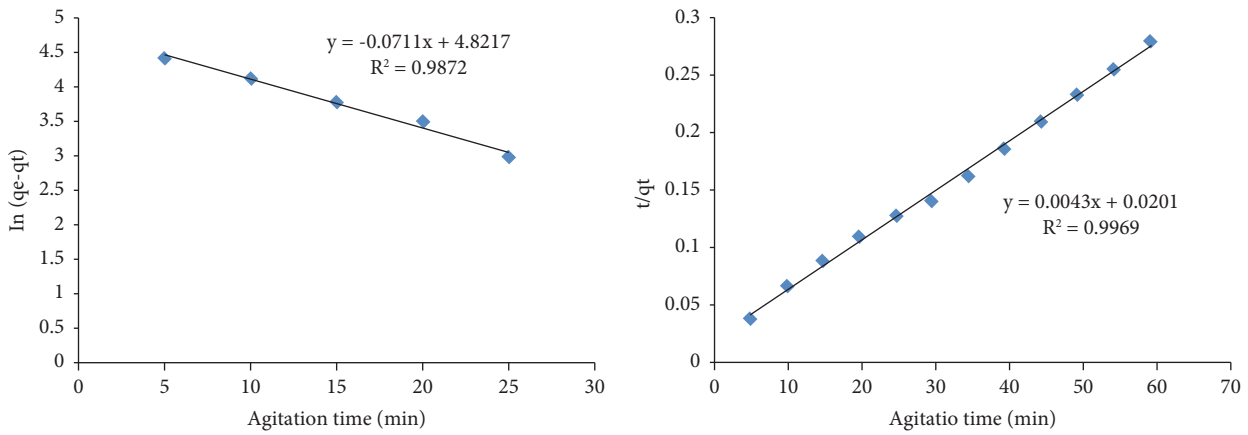

Figure 4: Continued.

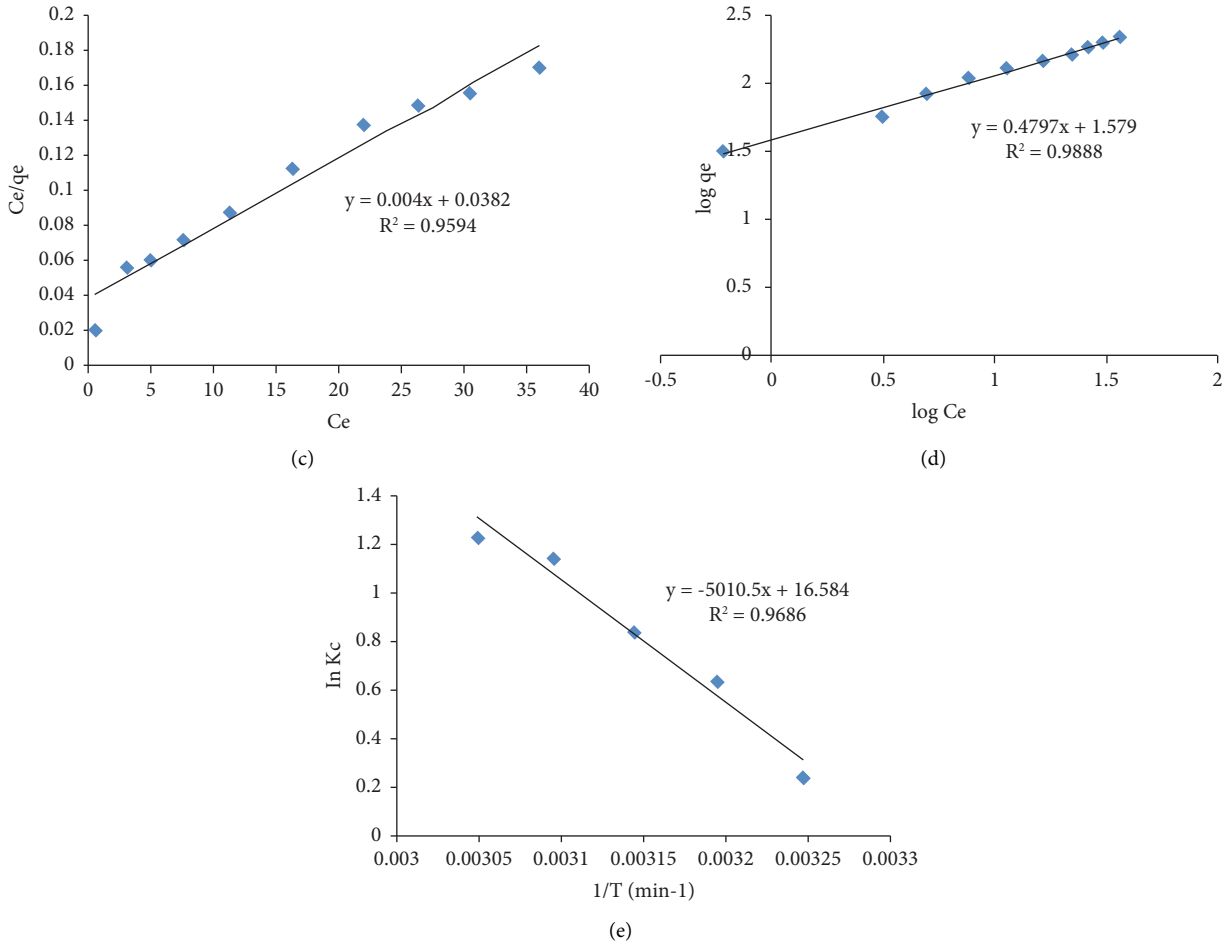

Figure 4: Kinetics, isotherms, and thermodynamics of adsorption of CR dye by Cu/ZnONPs: (a) pseudo-first-order kinetics; (b) pseudo-second-order kinetics; (c) Langmuir isotherm model; (d) Freundlich isotherm model; (e) thermodynamics.

Table 5: Kinetic parameters of adsorption of CR dye by Cu/ZnO NPs.

Kinetics of adsorption	q_e (mg/g)	R^2
Pseudo-first-order	124.08	0.987
Pseudo-second-order	250	0.996

indicate the endothermic nature and increase in the degree of randomness at the solid-solution interface during the adsorption process, respectively [19].

3.7. Adsorption Mechanism. The kinetics, isotherms, and thermodynamics of the adsorption data suggested that the chemical interaction between CR and the synthesized adsorbent was important in CR removal. The solution pH effect, on the other hand, demonstrated that electrostatic attraction was the primary mechanism for CR adsorption to the adsorbents. The aromatic rings of the linker are believed to interact with the aromatic rings of the dye through the π-π stacking interaction. It should be highlighted that doping can aid in the production of additional OH radicals; hence, the produced nanocomposite has a high capacity for CR adsorption.

3.8. Stability of the Adsorbent. Leaching experiments are used to determine the stability of the composite adsorbent. The stability will be evaluated in acidic, neutral, and basic environments [34–36]. In 100 ml of HCl and NaOH solutions, one gram of the adsorbent Cu/ZnONP is added. After a 24-hr contact time, the dissolved copper level (mg/g) was determined by atomic absorption spectroscopy. The

Table 6: Thermodynamic parameters of adsorption of CR dye by Cu/ZnONPs at different temperatures.

T (K)	ΔG (J/mol)	ΔH (kJ/mol)	ΔS (J·mol/K)
308	−629.143	41.653	137.84
313	−1660.73		
318	−2227.1		
323	−3065.02		
328	−3354.92		

experiment was repeated three times, with the average value published. The experiment was conducted at various acidic and basic pH levels, namely, 3, 7, and 9. It has been identified that copper dissolution is slightly higher at acidic pH conditions in comparison with neutral and basic conditions. The adsorbent showed highest stability at pH = 9 and lowest stability at pH = 3.

4. Conclusions

In the current study, chemical precipitation was used to synthesize copper-doped zinc oxide nanoparticles, which were then examined using XRD, SEM, and FTIR analyses. XRD examination revealed that the Cu/ZnONPs particles were homogeneous in size. Cu/ZnONPs have a spherical form, as seen by SEM images. Synthesized Cu/ZnONPs were employed in an adsorption approach to remove CR dye from an aqueous solution. Furthermore, FTIR analysis revealed that the interaction with CR dye molecules changed or abolished the unique bonds seen in Cu/ZnONPs. Cu/ZnONPs were employed to remove CR dye, and RSM-CCD was used to explore process parameter optimization. The agitation period of 29.48 min, the Cu/ZnONP dosage of 0.301 g/L, the solution pH of 6.96, and the CR initial concentration of 90 mg/L resulted in a maximum CR adsorption of 94.14% and a desirability of 0.976. The highest adsorption capacity determined by Langmuir isotherm was 250 mg/g, which agrees with the experimental adsorption capacity of 213.04 mg/g. The adsorption kinetics was best characterized by the pseudo-second-order model. According to thermodynamic studies, the adsorption process was endothermic and spontaneous. The synthesized Cu/ZnONPs is a potential adsorbent for the adsorption of toxic dyes from water in large-scale operations due to their efficiency, mobility, and high surface area.

Data Availability

All the data are available within the article.

Conflicts of Interest

The authors declare that they have no conflicts of interest.

References

[1] P. P. Rath, S. S. Behera, B. Priyadarshini et al., "Influence of Mg doping on ZnO NPs for enhanced adsorption activity of Congo Red dye," *Applied Surface Science*, vol. 491, pp. 256–266, 2019.

[2] S. Supriya and S. Sathish, "Enhanced photocatalytic decolorization of Congo red dye with surface-modified zinc oxide using copper(II)-amino acid complex," *Inorganic and Nano-Metal Chemistry*, vol. 50, no. 3, pp. 100–109, 2019.

[3] M. M. Ba-Abbad, S. Mohd, Takriff, and AbdelbakiBenamor, "Synthesis and characterisation of Co2+ -incorporated ZnO nanoparticles prepared through a sol-gel method," *Advanced Powder Technology*, vol. 27, 2016.

[4] M. Sajjad, I. Ullah, M. I. Khan, J. Khan, and M. Yaqoob Khan, "Structural and optical properties of pure and copper doped zinc oxide nanoparticles," *Results in Physics*, vol. 9, 2018.

[5] Y. Y. Chan, Y. L. Pang, S. Lim, C. W. Lai, A. Z. Abdullah, and W. C. Chong, "Biosynthesized Fe- and Ag-doped ZnO nanoparticles using aqueous extract of Clitoria ternatea Linn for enhancement of sonocatalytic degradation of Congo red," *Environmental Science and Pollution Research*, vol. 27, no. 28, pp. 34675–34691, 2020.

[6] S. R. Mousavi, M. Asghari, and N. M. Mahmoodi, "Chitosan-wrapped multiwalled carbon nanotube as filler within PEBA thin film nanocomposite (TFN) membrane to improve dye removal," *Carbohydrate Polymers*, vol. 237, 2020.

[7] N. M. Mahmoodi, M. Bashiri, and S. J. Moeen, "Synthesis of nickel–zinc ferrite magnetic nanoparticle and dye degradation using photocatalytic ozonation," *Materials Research Bulletin*, vol. 47, no. 12, pp. 4403–4408, 2012.

[8] S. Mata, T. Punugoti, B. Sowjanya, V. Rao Poiba, and M. Vangalapati, "Synthesis of Cu/ZnO nanoparticles and its exploitation as a catalyst for the removal of Cetrimonium Bromide," *Advances in Materials and Processing Technologies*, vol. 8, 2021.

[9] G. Hitkari, P. Chowdhary, V. Kumar, S. Singh, and A. Motghare, "Potential of Copper-Zinc Oxide nanocomposite for photocatalytic degradation of Congo red dye," *Cleaner Chemical Engineering*, vol. 1, Article ID 100003, 2022.

[10] B. Sowjanya, U. Sirisha, A. Suhasini Juttuka, S. Matla, P. King, and M. Vangalapati, "Synthesis and characterization of zinc oxide nanoparticles: it's application for the removal of alizarin red S dye," *Materials Today: Proceedings*, vol. 62, no. 6, pp. 3968–3972, 2022.

[11] K. salehi, HiuaDaraei, P. Teymouri, B. Shahmoradi, and A. Maleki, "Cu-doped ZnO nanoparticle for removal of reactive black 5: application of artificial neural networks and multiple linear regression for modelling and optimization," *J. Desalination and water treatment*, vol. 57, pp. 1–7, 2015.

[12] P. P. Magar, V. S. Kadam, S. F. Mulla, A. V. Shaikh, and H. M. Pathan, "Copper and iron doped zinc oxide: chemical synthesis, characterization and their properties," *Journal of Materials Science: Materials in Electronics*, vol. 27, no. 12, pp. 12287–12290, 2016.

[13] A. K. Chauhan, N. Kataria, and V. Garg, "Green fabrication of ZnO nanoparticles using Eucalyptus spp. leaves extract and their application in wastewater remediation," *Chemosphere*, vol. 247, Article ID 125803, 2020.

[14] F. Zhang, X. Chen, F. Wu, and Y. Ji, "High adsorption capability and selectivity of ZnO nanoparticles for dye removal," *Colloids and Surfaces A: Physicochemical and Engineering Aspects*, vol. 509, pp. 474–483, 2016.

[15] N. Kataria, V. K. Garg, M. Jain, and K. Kadirvelu, "Preparation, characterization and potential use of flower shaped

Zinc oxide nanoparticles (ZON) for the adsorption of Victoria Blue B dye from aqueous solution," *Advanced Powder Technology*, vol. 27, no. 4, pp. 1180–1188, 2016.

[16] A. Meng, J. Xing, Z. Li, and Q. Li, "Cr-doped ZnO nanoparticles: synthesis, characterization, adsorption property, and recyclability," *ACS Applied Materials & Interfaces*, vol. 7, no. 49, pp. 27449–27457, 2015.

[17] M. N. Zafar, Q. Dar, F. Nawaz, M. N. Zafar, M. Iqbal, and M. F. Nazar, "Effective adsorptive removal of azo dyes over spherical ZnO nanoparticles," *Journal of Materials Research and Technology*, vol. 8, no. 1, pp. 713–725, 2019.

[18] P. Raju, D. Deivatamil, J. Martin Mark, and J. P. Jesuraj, "Antibacterial and catalytic activity of Cu doped ZnO nanoparticles: structural, optical, and morphological study," *Journal of the Iranian Chemical Society*, vol. 19, no. 3, pp. 861–872, 2022.

[19] K. V. Karthik, A. V. Raghu, K. R. Reddy et al., "Green synthesis of Cu-doped ZnO nanoparticles and its application for the photocatalytic degradation of hazardous organic pollutants," *Chemosphere*, vol. 287, Article ID 132081, 2022.

[20] A. Gnanaprakasam, V. M. Sivakumar, and M. Thirumarimurugan, "A study on Cu and Ag doped ZnO nanoparticles for the photocatalytic degradation of brilliant green dye: synthesis and characterization," *Water Science and Technology*, vol. 74, no. 6, pp. 1426–1435, 2016 Sep.

[21] N. Manivannan, A. Sycheva, F. Kristály, G. Muránszky, and P. Baumli, "Structural differences and adsorption behaviour of alkaline metals doped zinc oxide nanoparticles," *Scientific Reports*, vol. 12, no. 1, p. 2292, 2022.

[22] C. Klett, A. Barry, I. Balti, P. Lelli, F. Schoenstein, and N. Jouini, "Nickel doped Zinc oxide as a potential sorbent for decolorization of specific dyes, methylorange and tartrazine by adsorption process," *Journal of Environmental Chemical Engineering*, vol. 2, no. 2, pp. 914–926, 2014.

[23] M. Saruchi, M. Sharma, M. R. Hatshan, V. Kumar, and A. Rana, "Sequestration of Eosin dye by magnesium (II)-Doped zinc oxide nanoparticles: its kinetic, isotherm, and thermodynamic studies," *Journal of Chemical and Engineering Data*, vol. 66, no. 1, pp. 646–657, 2021.

[24] L. Khezami, K. K. Taha, I. Ghiloufi, and L. El Mir, "Adsorption and photocatalytic degradation of malachite green by vanadium doped zinc oxide nanoparticles," *Water Science and Technology*, vol. 73, no. 4, pp. 881–889, 2016.

[25] M. Venkata Ratnam, M. Vangalapati, K. Nagamalleswara Rao, and K. Ramesh Chandra, "Efficient removal of methyl orange using magnesium oxide nanoparticles loaded onto activated carbon," *Bulletin of the Chemical Society of Ethiopia*, vol. 36, no. 3, pp. 531–544, September 2022.

[26] N. R. Kanidarapu, S. Feroz, and M. Vangalapati, "Response surface modelling of the removal of methyl orange dye from aqueous solution using magnesium oxide nanoparticles immobilized on chitosan," *Iranian Journal of Chemistry and Chemical Engineering (International English Edition)*, vol. 41, 2021.

[27] S. J. Charde, S. S. Sonawane, A. P. Rathod, S. H. Sonawane, N. G. Shimpi, and V. R. Parate, "Copper-doped zinc oxide nanoparticles: influence on thermal, thermo mechanical, and tribological properties of polycarbonate," *Polymer Composites*, vol. 39, no. S3, pp. E1398–E1406, 2018.

[28] M. Oveisi, M. Bakhtiari, B. Hayati, A. Bagheri, and S. Rahimi, "Environmentally friendly ultrasound-assisted synthesis of magnetic zeolitic imidazolate framework - graphene oxide nanocomposites and pollutant removal from water," *Journal of Molecular Liquids*, vol. 282, 2019.

[29] N. M. Mahmoodi, M. Ghezelbash, M. Shabanian, F. Aryanasab, and M. R. Saeb, "Efficient removal of cationic dyes from colored wastewaters by dithiocarbamate-functionalized graphene oxide nanosheets: from synthesis to detailed kinetics studies," *Journal of the Taiwan Institute of Chemical Engineers*, vol. 81, pp. 239–246, 2017.

[30] F. Hosseini, S. Sadighian, H. Hosseini-Monfared, and N. M. Mahmoodi, "Dye removal and kinetics of adsorption by magnetic chitosan nanoparticles," *Desalination and Water Treatment*, vol. 57, no. 51, pp. 24378–24386, 2016.

[31] D. Kurumilla, M. Vangalapati, and M. Venkata Ratnam, "Extraction of catechins from aegle marmelos fruit pulp: statistical optimization using response surface methodology and artificial neural networks," *International Journal of Chemical Engineering*, vol. 2022, Article ID 4933015, 12 pages, 2022.

[32] E. Matei, C. Predescu, A. Berbecaru, A. Predescu, and R. Trusca, "Leaching tests for synthesized magnetite nanoparticles used as adsorbent for metal ions from liquid solutions," *Digest Journal of Nanomaterials and Biostructures*, vol. 6, no. 4, pp. 1701–1708, 2011.

[33] K. Saravanakumar, B. Sankari Naveen Prasad, R. Senthilkumar, D. Mogili Reddy Prasad, and D. Venkatesan, "Single and competitive sorption potential of date seed-derived biochar during removal of lead (Il) and cadmium (Il) ions," *Environmental Progress & Sustainable Energy*, vol. 40, 2021.

[34] K. Saravanakumar, R. Senthilkumar, D. Mogili Reddy Prasad, B. Sankari Naveen Prasad, S. Manickam, and V. Gajendiran, "Batch and column arsenate sorption using turbinaria ornate seaweed derived biochar: experimental studies and mathematical modelling," *ChemistrySelect*, vol. 5, pp. 1–9, 2020.

[35] D. M. Reddy Prasad, L. Govindarajan, K. Saravanakumar, and B. S. Naveen Prasad, "Synthesis of green marine algal-based biochar for remediation of arsenic(V) from contaminated waters in batch and column mode of operation," *International Journal of Phytoremediation*, vol. 22, 2019.

[36] D. M. Reddy Prasad, L. Govindarajan, K. Saravanakumar, and B. S. Naveen Prasad, "Improved sorption of reactive black 5 by date seed-derived biochar: isotherm, kinetic, and thermodynamic studies," *Separation Science and Technology*, vol. 54, no. 15, pp. 2351–2360, 2019.